The functional form of the general solution implies the following equality:

$$\partial\delta/\partial t = -c(\partial\delta/\partial y) \quad (6)$$

Substituting the boundary conditions, and solving for the suspension-line tension at the deployment bag mouth gives

$$T_B = K'n(V_R - u)/c \quad (7)$$

An approximate expression for the snatch force is obtained from Eqs. (1) and (7). The suspension-line tension is eliminated from Eq. (7) using Eq. (1) and the resulting quadratic solved for the steady-state unfurling rate. The corresponding tension (snatch force) is found by substituting the steady-state unfurling rate in Eq. (1). This result can be expressed as

$$P = nK'[\{1 - (1 + 4A)^{1/2}\}/(2r) + V_{Rle}/c] \quad (8)$$

where

$$A = r[V_{Rle}/c - F_{re}/(nK')], r = m_c'/(nm_{sl}')$$

Results and Discussion

The present snatch-force theory was compared with flight data obtained during the Planetary Entry Parachute Program (PEPP) and the Supersonic Planetary Entry Decelerator Program (SPED).[4] For these calculations, the deployment velocity at line extension was determined by numerical integration of the general equations describing the dynamics of lines-first deployments.[5] The unfurling resistance was neglected. The elastic modulus of the suspension lines was determined from static test data. The linear mass density of the canopy skirt was determined by dividing the mass of the skirt hem (including the tape reinforcement, the overlapping radial tapes, and an appropriate amount of canopy cloth) by the width of the hem. Calculated values for these parameters are summarized in Table 1. The resulting snatch-force predictions using Eq. (8) are compared with flight data in Fig. 2. Also shown in this figure is a comparison between the flight data and the "handbook method"[1] for calculating snatch force. As can be seen, the present method significantly improves the prediction accuracy. The remaining disagreement between theory and flight is thought to be the result of nonideal packing and construction, angle of incidence between the deployment bag and the suspension lines, undetermined unfurling resistance, and nonlinearities in the elastic properties of the suspension lines.

Concluding Remarks

Snatch force, for a lines-first deployment, has been related to the increase in linear mass density of the unfurling decelerator as the canopy skirt emerges from the deployment bag. An approximation to the snatch force was obtained from a steady-state solution to the wave equation which approximates the linear elastic behavior of the suspension lines. Prediction accuracy using the present theory was significantly better than results obtained by applying the canopy-first theory of the "handbook method."

References

[1] "Performance of and Design Criteria for Deployable Aerodynamic Decelerators," ASD-TR-61-579, Dec. 1963, U.S. Air Force.

[2] Heinrich, H. G., "Parachute Snatch Force," *Aerodynamic Deceleration 69*, Lecture Notes, 1969, Chap. 5, Univ. of Minnesota, Minneapolis, Minn.

[3] Schutt, P., "Die Berechnung der Streckstosskraft von Fallschirmen," *Fallschirmtechnik und Bergungssystem*, DLR Mitt. 69-11, Sept. 1969, pp. 74–95.

[4] Whitlock, C. H. and Bendura, R. J., "Inflation and Performance of Three Parachute Configurations From Supersonic Flight Tests in a Low Density Environment," TN D-5296, 1969, NASA.

[5] Huckins, E. K., III, "Techniques for Selection and Analysis of Parachute Deployment Systems," TN D-5619, 1970, NASA.

Effect of Asymmetrical Flow from Trailblazer Flight Measurements

R. DeVore,* R. Caldecott,† and J. D. Lee‡
The Ohio State University, Columbus, Ohio

A MAJOR problem in predicting r.f. (radio frequency) conditions in a re-entry environment is the extreme complexity of the flow in all but the simplest of situations. The difficulties may arise from a number of causes: vehicle shape, nonequilibrium effects, and the addition of chemical additives to the flow, either deliberately or as a byproduct of ablation, are some of the principal ones. In a recent flight experiment a payload, consisting basically of a 9°-half-angle cone with a cylindrical VHF monopole antenna at the nose, was flown aboard a Trailblazer vehicle. Data received by various ground stations were in good agreement, but there was considerable fluctuation of the received signal strength. A detailed analysis of the flight showed that maximum signal attenuation occurred when the leeward flow was between the on-board VHF transmitter and the ground-based VHF receivers. The envelope of the received signal is shown in Fig. 1. From 407 sec $< t <$ 418 sec the vehicle was undergoing a coning motion with the angle of attack α decreasing from a maximum of 8° to a minimum of 2°. The re-entry velocity was essentially constant at 16,800 fps. The vehicle spin was stabilized at ~3 rps.

Based upon an axisymmetric inviscid flow calculation (stream tube method), it was found that except for a few db all attenuation was due to the thermal boundary layer on the antenna.[1] The gross validity of the inviscid flow calculations was substantiated by schlieren photographs of $\frac{1}{4}$-scale-model wind-tunnel tests, with $\alpha = 4°$. The purpose of this Note is to account for the windward-leeward variation in the transmitted VHF signal.

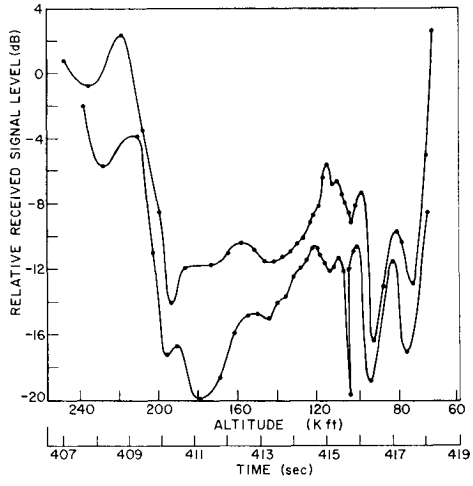

Fig. 1 Average VHF signal recorded by three ground based receivers (lower curve leeward aspect, upper curve windward aspect, abscissa linear with time).

Received November 23, 1970; revision received December 28, 1970. The work reported in this paper was supported in part by Contract F33615-69-C-1205 between Air Force Avionics Laboratory, Wright-Patterson Air Force Base and The Ohio State University Research Foundation.

* Associate Professor and Supervisor, ElectroScience Laboratory, Department of Electrical Engineering.

† Associate Supervisor, ElectroScience Laboratory, Department of Electrical Engineering.

‡ Professor and Director, Aeronautical and Astronautical Research Laboratory, Department of Aeronautical and Astronautical Engineering. Member AIAA.

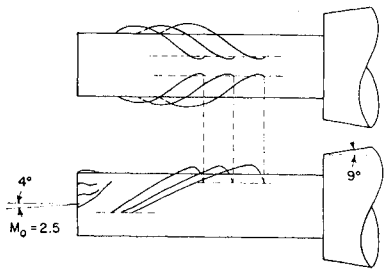

Fig. 2 Sketches of detached boundary flow (laminar).

Antenna Performance

The flight antenna is a rather complicated radiating structure—a half wave dipole with a cylinder forearm and a conical aftarm. Its behavior in a conducting medium (the electron concentration in a time varying flow) cannot be fully and simply described. The antenna-plasma model which suggests itself is that of a dipole imbedded in an infinite, uniform and cold plasma column. The ratio of the power radiated normal to the cylinder to the power radiated in the same direction without plasma is[1]

$$P = \frac{\left(\frac{2}{\pi k_0 b}\right)^2 \left|\frac{J_0(k_0 a \epsilon_p^{1/2})}{J_0(k_0 a)}\right|^2 \left|\frac{F(I_{\epsilon_p})}{F(I_1)}\right|^2}{\left|\epsilon_p^{1/2} J_1(k_0 b \epsilon_p^{1/2}) H_0^{(1)}(k_0 b) - J_0(k_0 b \epsilon_p^{1/2}) H_1^{(1)}(k_0 b)\right|^2} \quad (1)$$

where a is the cylinder radius, b is the radius of the cylinder and the plasma column, the J's and H's are the appropriate Bessel functions, and k_0 is the free space wavenumber. The plasma is represented by the relative permittivity,

$$\epsilon_p = 1 - (\omega_p/\omega)^2(1 + i\nu/\omega)^{-1} \quad (2)$$

where ν is the collision frequency; the electron plasma frequency $\omega_p = 5.64 \times 10^4 n_e^{1/2}$, where n_e is the electron density (cm^{-3}); and ω is the angular frequency of radiation. The antenna-plasma interaction of Eq. (1), $F(I_{\epsilon_p})/F(I_1)$ is for simplicity set equal to unity. This implies that the plasma environment does not affect the antenna current—an assumption that is not entirely valid. The direction of radiation in Eq. (1) is taken as normal to the cylinder, a condition that existed approximately for the re-entry period.

Thus for tractability, the physical radiating structure and flow have been replaced by a highly simplified model. If only the inviscid flow were considered in evaluating Eq. (1), the power received would decrease monotonically from 0 db at 240 kft to −4 db at 120 kft, based on calculation of the inviscid flow by the stream-tube method with the cylinder at $\alpha = 0$.

Investigation of the Boundary Layer

The attenuation variations shown in Fig. 1 cannot be fully described by an axisymmetric flow due to the coning motion at angle of attack. There has been recent interest[2,3] in spinning slender bodies of revolution undergoing coning motion at an angle of attack. From these results it appears that due to the relatively small α's involved, the effect of the coning motion would not significantly affect the shock-layer heating, although some flow distortion obviously occurs. Consequently the effect of coning has been neglected.

Tests were conducted on a $\frac{1}{4}$-scale model at $\alpha = 4°$ at Mach 2.5 and free-stream unit Reynolds numbers (Re) of 0.6×10^6 ft^{-1} and 3.1×10^6 ft^{-1}. Schlieren photographs showed the windward and leeward shock structure to be virtually indistinguishable for both conditions. From this geometrical similarity it was concluded that the attenuation variation was a boundary-layer effect.

Oil-streak photographs of the leeward flow were then taken for both freestream Reynold numbers to ascertain the nature of the boundary-layer flow. From these photographs a sketch of the indicated detached flow is shown in Fig. 2 for a Re of 0.6×10^6 ft^{-1}. The boundary layer detaches below the midplane on the windward side and reattaches on the leeward side in a rolling vortex motion, typical for bodies and small rings at low Re. The boundary layer also separates at the periphery of the face of the cylinder and then reattaches. No attempt was made to investigate the nature of the boundary-layer flow between the leeward reattachment lines or in the vicinity of the cone base.

Based upon a conical flow and the flight profile the transition point, from a laminar to a turbulent boundary-layer separation, occurs somewhere below 70,000 ft. Consequently, for almost the entire re-entry period shown in Fig. 1, the detached flow will be grossly similar to that shown in Fig. 2.

For a Re $= 3.1 \times 10^6$ ft^{-1}, the oil-streak photographs showed that boundary-layer transition had occurred. The separation line had moved downstream, and an interesting vortex pattern had formed behind the separation line on the leeward side of the cylinder. However, this condition prevailed only during the terminal phase of the re-entry period.

Although many of the details of the boundary-layer flow on a blunt cylinder at angle of attack are unknown, qualitatively the windward portion can be described as somewhat hotter and thinner than the zero-α case. On the other hand, the leeward side, which is fed by the windward cross flow, will be considerably thicker and is composed of a rather complex vortex structure.

Discussion

Now let us attempt to explain the attenuation variation due to aspect. The antenna-plasma model of Eq. (1) assumes a finite dipole imbedded in a uniform plasma column. The flow is assumed not to affect the dipole current distribution. Thus the relative radiated power is mainly affected by the electron density about the antenna and secondarily the average electromagnetic thickness d of the boundary layer. Thermal boundary-layer calculations were made to obtain an estimate of the electron concentrations and d. With these nominal values, Eq. (1) was evaluated with electron concentration and d as variables. The VHF frequency was 231.4 MHz, so all boundary-layer dimensions are very thin in terms of wavelength. The actual thin nonuniform layers

Table 1 Windward and leeward attenuation variations for flight experiment and calculations

Altitude, kft	Flight experiment: Attenuation, db			Calculations[a]				
					Windward		Leeward	
	Windward	Leeward	Variation	ω_p/ω	d, in.	Attenuation, db	d, in.	Attenuation, db	Difference, db
200	8.5	14.5	6.0	10.5	0.15	8.9	0.60	15.0	6.1
193	14.0	17.0	3.0	12.8	0.15	11.2	0.60	18.4	7.4
180	12.0	20.0	8.0	15.6	0.09	12.4	0.36	17.7	5.3
160	10.5	15.5	5.0	15.8	0.06	11.8	0.24	15.3	3.5
140	11.5	14.0	2.5	16.8	0.035	11.2	0.14	13.2	2.0
120	8.5	10.5	2.0	18.2	0.025	9.0	0.10	10.3	1.3
100	7.5	10.5	3.0	28.5	0.016	9.7	0.064	10.4	0.7

[a] d is an average electromagnetic thickness (in.) for the boundary layer on the cylinder.

are replaced with equivalent uniform thin layers for the purposes of evaluation. These equivalent layers are more of an average electromagnetic thickness rather than a velocity boundary layer as Eq. (1) is particularly sensitive to the plasma frequency ω_p, which is also an average value for the layer.

Based upon the equivalent antenna-plasma model, the calculations show the windward-leeward attenuation variations can be explained in terms of an approximately equal electron density (and plasma frequency, ω_p) on both sides of the cylinder. The leeward side d is roughly four times that on the windward side, as shown in Table 1. The effective thickening is due to the complex separated vortex pattern rolling over from the windward side.

References

[1] DeVore, R. and Caldecott, R., "Radiation by a VHF Dipole Imbedded in its Plasma Sheath," *Proceedings of Conference on Environmental Effects on Antenna Performance*, Vol. II, edited by J. R. Wait, Environmental Science Services Administration, July 1969 (available DDC).

[2] Tobak, M., Schiff, L. B., and Peterson, V. L., "Aerodynamics of Bodies of Revolution in Coning Motion," *AIAA Journal*, Vol. 7, No. 1, Jan. 1969, pp. 95–99.

[3] Kuhn, G. D., Spangler, S. B., and Nielsen, J. N., "Theoretical Study of Vortex Shedding from Bodies of Revolution Undergoing Coning Motion," CR-1448, Oct. 1969, NASA.

Reinforced Composite Materials with Curved Fibers

FARHAD TABADDOR* AND C. H. CHEN†
The B. F. Goodrich Co., Akron, Ohio

Introduction

THE initial fiber misalignment in a unidirectional reinforced composite can affect, considerably, the mechanical properties in comparison to an ideal reinforced composite with fibers, being assumed straight. The subject has been considered by a number of investigators. Among them, Tarnopolsky et al.,[1] used a mechanics of material approach to obtain the axial Young's modulus of a fiber-reinforced composite ply with fiber misalignment only in the plane of the ply. They assumed that the fiber misalignment is uniform and symmetric with respect to the longitudinal axis, so that the fiber path can be represented reasonably well by a sinusoidal curve (Fig. 1a). They then considered a segment of length dx (Fig. 1b) and obtained the Young's modulus in x direction of this segment in terms of the properties of straight-fiber composite by using transformation formula. This Young's modulus of the segment was then integrated over a length of a period to yield a closed form expression for the apparent Young's modulus in x direction. It is reported in Ref. 1 that good agreement was obtained between theory and experiment. Other experimental verification on the effect of curved fibers can be found in Ref 2.

In this Note, using the result for Young's modulus obtained in Ref. 1, the one-dimensional stress-strain relation of a composite with curved fiber will be derived, and the effect of misalignment on this stress-strain relation will be studied.

Basic Relations

We will consider the two-dimensional problem of the unidirectional reinforced composite with curved fibers subjected to unidirectional loading. The fiber, as shown in Fig. 1a, is

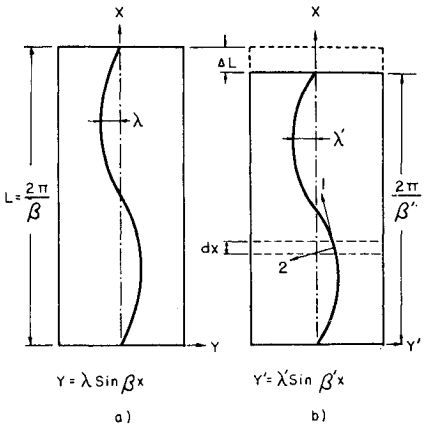

Fig. 1 Basic element a) before and b) after deformation.

assumed to have sinusoidal misalignment, expressed by

$$y = \lambda \sin\beta x \tag{1}$$

where y measures the deviation of a typical fiber from the average position, and λ and $\beta = 2\pi/L$ are amplitude and frequency of misalignment, respectively. Figure 1b shows the same fiber after deformation as a result of loading in x direction. Upon the application of the load, the material deforms, and the reinforcing fiber would assume a new sinusoidal form given by

$$y = \lambda' \sin\beta' x \tag{2}$$

The Young's modulus in x direction of a composite with fibers having the path of Eq. (2) is given, according to Ref. 1, as

$$\frac{1}{E_x} = \frac{1}{2}\left(\frac{1}{E_{11}} - \frac{1}{G_{12}} + \frac{2\nu_{12}}{E_{11}} + \frac{1}{E_{22}}\right)[2 + (\lambda'\beta')^2] \times [1 + (\lambda'\beta')^2]^{-3/2} + \left(\frac{1}{G_{12}} - \frac{2\nu_{12}}{E_{11}} - \frac{2}{E_{22}}\right) \times [1 + (\lambda'\beta')^2]^{-1/2} + \frac{1}{E_{22}} \tag{3}$$

where E_{11}, E_{22}, G_{12}, and ν_{12} are the axial Young's modulus, transverse Young's modulus, longitudinal shear modulus, and Poisson's ratio, respectively, of unidirectional composite with straight fibers. These quantities can be evaluated by various micromechanical theories if the properties of constituent materials and the fiber volume ratio (v) are known. If in addition the quantity $\lambda'\beta'$ can be related to the given initial conditions of λ, β and to the amount of strain ϵ, then E_x can be evaluated from Eq. (3). Thus we have relation of E_x vs ϵ, which usually is a nonlinear in nature. Knowing E_x corresponding to a particular value of ϵ, the stress required to produce that strain is given in conventional manner as

$$\sigma_x = E_x\epsilon \tag{4}$$

which gives us, in general, nonlinear stress-strain relation of a composite under our consideration.

Let us observe from Eq. (2) that the amplitude and frequency of misalignment appear as a product and therefore

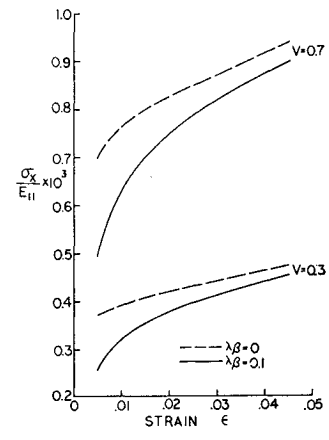

Fig. 2 Nondimensional stress-strain relations for reinforced composites with ν_m = 0.49, ν_f = 0.33, and G_f/G_m = 3000.

Received October 1, 1970.

* Senior Engineering Scientist.

† Senior Engineering Scientist. Member AIAA.